Lamellar polymer–Li_xMoO_3 nanocomposites *via* encapsulative precipitation

Lei Wang,[a] Jon Schindler,[b] Carl R. Kannewurf[b] and Mercouri G. Kanatzidis*[a]

[a]*Department of Chemistry and the Center for Fundamental Materials Research, Michigan State University, East Lansing, Michigan 48824, USA*

[b]*Department of Electrical Engineering and Computer Science, Northwestern University, Evanston, Illinois 60208, USA*

With Li_xMoO_3 ($x = 0.31$–0.40) as a host material, a new family of polymer–molybdenum bronze nanocomposites has been synthesized using an exfoliation/encapsulation methodology. Nanocomposites with poly(ethylene oxide), poly(ethylene glycol), poly(propylene glycol), poly(vinylpyrrolidinone), methyl cellulose, polyacrylamide, and nylon-6 were prepared and characterized by thermal gravimetric analysis (TGA), differential scanning calorimetry (DSC), powder X-ray diffraction, FTIR spectroscopy, UV–VIS spectroscopy, variable-temperature ^{7}Li and ^{13}C solid-state NMR spectroscopy and magnetic susceptibility measurements. The electrical conductivity of these materials lies in the range from 10^{-2} to 10^{-7} S cm^{-1}, and decreases as the interlayer separation increases. The intercalated polymer imparts both mechanical strength and ease of processing to these materials. The water-soluble polymer–Li_xMoO_3 nanocomposites can be cast into films and other shapes, which may provide opportunities for applications. Factors affecting the intercalation reaction and the structure of nanocomposites, such as variations in the preparation procedure, the polymer molecular mass and the annealing behaviour of the products are discussed.

The investigation of polymer–inorganic nanophase composites is motivated by many reasons, including the need for novel electronic anisotropic materials, better performing battery cathode materials, functionalized structural materials with superior mechanical properties, hierarchical materials, and systems in which to study polymer orientation, epi- and endo-taxy and polymer/inorganic surface interactions.[1–28] Polymer-based nanocomposites have been reported with layered silicates (*e.g.* montmorillonite, hectorite, *etc.*),[1–9] FeOCl,[10] V_2O_5,[11–13] MoO_3,[14,15,26,27] layered metal phosphates,[16–20] MS_2 (M = Mo,[21–24,26] Ti[24]), layered metal phosphorus chalcogenides (MPS_3)[25–27] and layered double hydroxides.[28] The most common methods of preparing polymer–inorganic nanocomposites are (*a*) by monomer intercalation followed by polymerization, (*b*) by *in situ* intercalative polymerization, (*c*) by direct insertion and (*d*) by encapsulative precipitation from solutions of exfoliated lamellar solids. The last two methods give polymer–inorganic nanocomposites in which the molecular masses and nature of the polymers can be decided before intercalation. Encapsulative precipitation has been applied with V_2O_5,[11*a*–*c*,12] MoO_3,[14*a*–*c*,26] MoS_2,[22*b*,*c*,23,24,26] WS_2,[29] and TiS_2,[24] in combination with various polymers.

MoO_3 is one of the layered metal oxides which shows reversible Li ion insertion properties which are relevant to rechargeable Li batteries.[30,31] In intercalative electrodes of rechargeable batteries, ion conductivity is very important. Other solid-state ionic applications such as electrochromic devices also need good ion conductivity. Polymer–inorganic nanocomposites should exhibit fast ion conduction[8] and introduction of a polymer with affinity for Li ions between the sheets of MoO_3 could improve its performance as an intercalative electrode.

Polymer insertion into MoO_3 has been reported previously, namely, with a polymeric ionomer,[14*a*,*b*] with PEO[14*c*,26] and with polyaniline.[14*d*,15,27] This research develops further the polymer intercalation chemistry associated with MoO_3 and introduces a new family of polymer–Li_xMoO_3 nanocomposites. Nanocomposites with poly(ethylene oxide) (PEO), poly(ethylene glycol) (PEG), poly(propylene glycol) (PPG), poly(vinylpyrrolidinone) (PVP), methylcellulose (MCel), polyacrylamide (PAM) and nylon-6 (PA6) are reported here. These nanocomposites were characterized by thermal gravimetric analysis (TGA), differential scanning calorimetry (DSC), powder X-ray diffraction, FTIR and solid-state UV–VIS spectroscopy, variable-temperature solid-state ^{7}Li and ^{13}C NMR spectroscopy, magnetic susceptibility measurements and electrical conductivity measurements.

Experimental

Materials and methods

Reagents. PEO (5000000), PEO (100000), PEG (10000), PEG (2000), PEG (400), PPG (1000), PVP (10000), MCel (63000), PAM (5000000), PA-6 (10000) and $LiBH_4$ were purchased from Aldrich Chemical Company, Inc. After the polymers were dissolved, the polymer solutions were filtered to remove insoluble polymer residues. MoO_3 (99.95%) was purchased from Johnson Matthey. Anhydrous diethyl ether (99.0%), 2,2,2-trifluoroethanol (99%), acetonitrile (99.5%) isopropyl alcohol (99.9%) and absolute ethanol were from Columbus Chemical Industries Inc., Lancaster Synthesis Inc., EM Science Inc., Mallinckrodt Chemical Inc. and Quantum Chemical Company respectively. No further purification was applied to the chemicals above. Water used in the reactions was distilled water provided by the Department of Chemistry of MSU, and was degassed by bubbling nitrogen for 30 min before use.

Synthesis of Li_xMoO_3 ($0.30 < x < 0.40$). Commercial MoO_3, used as the starting material, was fired in an open quartz vial in the air at 600 °C for 36 h during which the crystallite size of MoO_3 remarkably increased. This MoO_3 was used to react with $LiBH_4$ to prepare the lithium molybdenum bronze.[32] In a typical reaction, 0.1 mol of MoO_3 was reacted with 0.04 mol of $LiBH_4$ in 80 ml diethyl ether for 24 h, under a nitrogen atmosphere. The product was collected by filtration, washed with ether and dried *in vacuo*. The yield was >98%. The lithium molybdenum bronze was thereafter stored in a nitrogen dry-box. The X-ray powder diffraction pattern can be indexed on the basis of an orthorhombic cell similar to that of MoO_3 but expanded along the stacking (*a*-axis) direction, with $a = 16.528$ Å, $b = 3.775$ Å and $c = 3.969$ Å. The d_{hkl}-spacings (Å) are: 8.27_{200} (vs), 4.132_{400} (s), 3.578_{201} (m), 3.434_{210} (m), 2.755_{600} (w), 2.453_{311} (m) and 2.372_{411} (m).

The amount of lithium in the bronze was analysed by TGA under oxygen flow, heating up to 650 °C, and by elemental analysis which was accomplished by Oneida Research Services, Inc., Whitesboro, New York. Elemental analysis of Li in the

molybdenum bronze was done by ion chromatography, while Mo was measured by X-ray fluorescence.

Preparation of polymer–Li_xMoO_3 nanocomposites. The Li_xMoO_3 was exfoliated in degassed water by 5 min of sonication, to form a suspension with a concentration of 5 g l^{-1}. This suspension was added dropwise into a stirred polymer solution of the same volume, which contained five times excess of polymer (per repeat unit) to MoO_3 and the mixture was stirred for 2 days under a nitrogen atmosphere. The nanocomposites formed were isolated in different ways according to their behaviour in solution. Nanocomposites of methylcellulose, polyacrylamide and nylon-6 precipitated and were collected by filtration. Those containing MCel and PAM were washed with water, while the nanocomposites of PA6 were washed with trifluoroethanol. Nanocomposites with poly(ethylene oxide), poly(ethylene glycol), poly(propylene glycol) and poly(vinylpyrrolidinone) remained in colloidal form and were isolated by pumping off the water to dryness. The dried material was stirred in an appropriate solvent for several hours to dissolve the extraneous polymer. The solid product was filtered and was washed again with the solvent. The solvents used to process the products are listed in Table 1. The products were pumped to dryness and stored in a nitrogen atmosphere.

Instrumentation

X-Ray powder diffraction patterns were obtained on a Rigaku Ru-200B X-ray diffractometer equipped with graphite-monochromated Cu-Ka radiation. A scanning speed of 1° min^{-1} was chosen. TGA was performed with a Shimadzu TGA-50 instrument under a nitrogen or oxygen flow at a rate of 46 ml min^{-1} and the heating rate was 10 °C min^{-1}. DSC was carried out on a Shimadzu DSC-50 instrument under a nitrogen flow at a rate of 20 ml min^{-1}. The heating and cooling rates were 5 °C min^{-1}. Sample cells were made of aluminium and were annealed at 450 °C in nitrogen after they were cleaned. Samples were sealed in cells under a nitrogen atmosphere before measurement. IR spectra were collected on a Nicolet IR/42 FTIR spectrometer at a resolution of 2 cm^{-1}. Generally 64 scans were obtained for samples as KBr pellets. Electronic transmission spectra were recorded with a Shimadzu UV-3101PC UV–VIS–NIR scanning spectrophotometer. Samples were dried as thin films on quartz slides.

Variable-temperature solid-state ^7Li and ^{13}C NMR measurements were taken on a 400 MHz Varian NMR instrument. Samples were loaded in a glove box under a nitrogen atmosphere. Magnetic susceptibility measurements were performed with a Quantum Design MPMS2 SQUID magnetometer. Samples were sealed in low-density polyethylene (LDPE) bags under a nitrogen atmosphere. Room-temperature conductivity measurements were performed on pressed sample pellets with a four-probe detector connected to a Keithley-236 source measuring unit. Variable-temperature dc electrical conductivity measurements were performed on compacted powders in pellet form with 60 and 25 mm gold wires used for the current and voltage electrodes, respectively. Measurements of the pellet cross-sectional area and voltage probe separation were made with a calibrated binocular microscope. Electrical conductivity data were obtained with a computer-automated system described elsewhere.[33]

Results and Discussion

Synthesis and characterization of Li_xMoO_3

The lithium molybdenum bronze exfoliates readily in water to form stable colloidal solutions, and this makes it an appealing candidate for polymer intercalation. The $LiBH_4$ route to Li_xMoO_3 is the best one to date in providing the material conveniently and in high yield. The previously reported method for $Li_x(H_2O)_yMoO_3$[34] involves one step to prepare $Na_x(H_2O)_yMoO_3$ and two steps to accomplish ion exchange and gives only 26% yield.† An additional advantage of the $LiBH_4$ method is that it is conducted in diethyl ether and so provides the anhydrous form of the molybdenum bronze. The Li_xMoO_3 product prepared in this fashion, though still crystalline, shows broader diffraction maxima than the precursor MoO_3. The Li insertion into MoO_3 is topotactic as evidenced by our ability to fully index the X-ray powder diffraction pattern of the product.

The amount of Li in Li_xMoO_3 was determined both by TGA and by direct elemental analysis. When the material is heated in an oxygen atmosphere to 650 °C, it gains 1.71 mass%, owing to a change from Li_xMoO_3 to Li_2O and MoO_3. This gain of mass is reproducible and corresponds to an x value of 0.31(3). On the other hand, the elemental analysis showed that the molybdenum bronze consisted of 1.64% Li and 56.39% Mo. This gives a ratio of Li to Mo of 0.4 : 1 corresponding to the molar ratio of $LiBH_4$ used in the lithiation reaction. It is of course possible that x varies slightly from sample to sample in the range $0.3 < x < 0.4$.

The lithium molybdenum bronze is metastable and undergoes an intense, irreversible and exothermic phase change

† Yield obtained by reproducing the experiment in ref. 34.

Table 1 Some chemical and structural characteristics of polymer–Li_xMoO_3 nanocomposites

nanocomposite	polymer M_W[a]	solubility	washing solvent	d-spacing/Å	expansion of gallery/Å	coherence length/Å
PEO–Li_xMoO_3	5 000 000	yes	MeCN	16.6	9.7	64
PEO–Li_xMoO_3	100 000	yes	MeCN	16.6	9.7	121
PEG–Li_xMoO_3	10 000	yes	MeCN	16.8	9.9	108
PEG–Li_xMoO_3	2000	yes	MeCN	13.8	6.9	72
				12.6–14.7	5.7–7.8	—[b]
PEG–Li_xMoO_3	400	yes	MeCN	13.5	6.6	111
				12.6	5.7	97
PPG–Li_xMoO_3	1000	yes	EtOH	17.2	10.3	113
				11.8	4.9	108
				18.0, 11.5	—	—[b]
MCel–Li_xMoO_3	63 000	no	H_2O	27.6	20.7	92
PVP–Li_xMoO_3	10 000	yes	Pr^iOH	38.6	31.7	154
PAM–Li_xMoO_3	5 000 000	no	H_2O	38.0	31.1	69
				33.8	26.9	80
				41.2	34.2	—[b]
PA6–Li_xMoO_3	10 000	no	CF_3CH_2OH	22.1	15.2	39
				16.8	9.9	26

[a]Polymer dissolved in water, except for PA6-10 000, dissolved in 2,2,2-trifluoroethanol. [b]Peaks too broad to obtain estimate.

at 356 °C, as detected by DSC (Fig. 1) and X-ray powder diffraction. The product appears to be a mixture of at least two unknown phases. As this mixture is heated to higher temperatures it undergoes additional phase changes yielding other new phases. The details of this reaction are currently under investigation.

Exfoliation and polymer encapsulation chemistry

The lithium molybdenum bronze described above can be readily exfoliated in water after several minutes of sonication. The exfoliated product forms supramolecular complexes with most water-soluble polymers. The complexes form solutions or precipitates in water, depending on the type and molecular mass of the polymers. We have encapsulated PEO, PEG, PPG, PAM, MCel and PVP inside the lithium molybdenum bronze to obtain lamellar nanocomposite materials.

Poly(ethyleneimine) (PEI) could not be successfully intercalated. Instead, the blue $Li_x(H_2O)_yMoO_3$ monolayer suspension decolorized and totally dissolved in the aqueous PEI solution. The same phenomenon occurred when ammonia was introduced in the $Li_x(H_2O)_yMoO_3$ suspension, suggesting that the PEI solution is too basic and attacks the MoO_3 lattice. Water-insoluble polymers were also tried, however of these, only PA6 was successfully intercalated. Details of the reactions are given in Table 1.

The existence of polymer chains between the layers of the lithium molybdenum bronze was verified by IR spectroscopy and X-ray powder diffraction. Fig. 2 shows a comparison of the IR spectra of a nanocomposite $Li_x(H_2O)_y(PVP)_zMoO_3$ and its components; from this, it is obvious that the vibrational spectrum of $Li_x(H_2O)_y(PVP)_zMoO_3$ is a combination of the vibrational spectrum of PVP and that of $Li_x(H_2O)_yMoO_3$. The positions of the vibrational peaks arising from the encapsulated PVP are close to those of pure PVP, while the positions of the peak due to the Mo=O stretch [for $Li_x(H_2O)_yMoO_3$] is shifted to higher wavenumbers, suggesting that the MoO_3 layers in the nanocomposite are slightly more oxidized.

The optical transmission absorption spectra of these macromolecular intercalates were examined. The dark-blue colour of these systems arises from the intense intervalence transitions associated with the Mo^{5+}–Mo^{6+} couple. These electronic transitions are broad and range from the IR region to the visible (Fig. 3) and are responsible for the electrical conductivity of these materials. The absorption at 286 nm arises from excitations across the band-gap from the O^{2-} p band to the Mo^{6+} d band and is present in all compounds including pristine MoO_3 and $Li_x(H_2O)_yMoO_3$. This is consistent with the expectation that host metal oxide structure is not disturbed upon intercalation.

The encapsulation of polymers inside the interlayer galleries

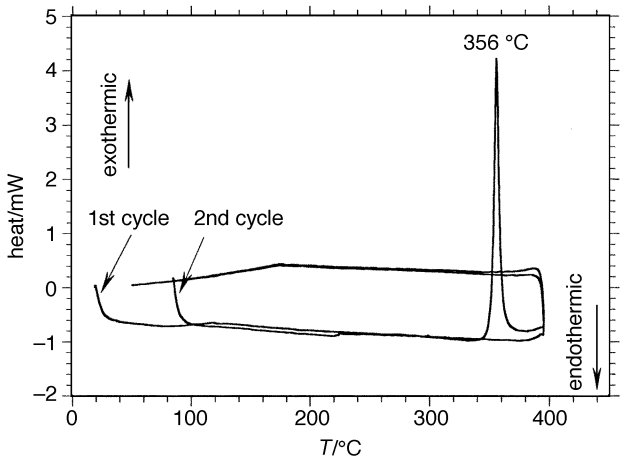

Fig. 1 DSC diagram of Li_xMoO_3

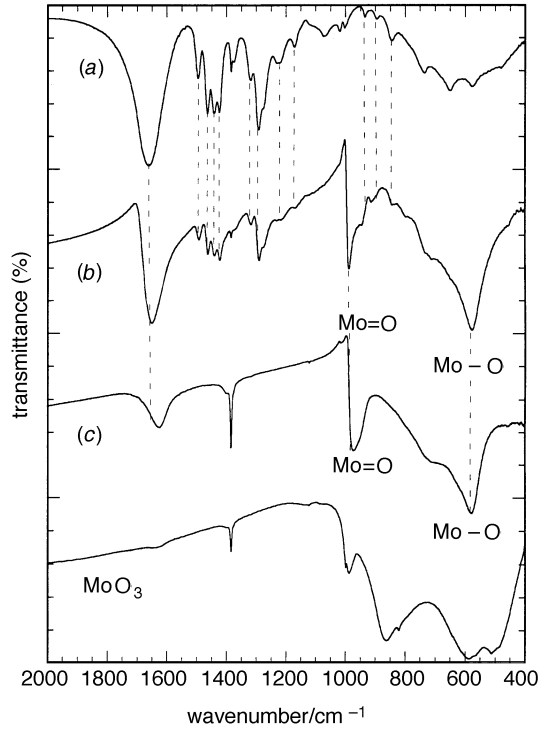

Fig. 2 IR spectra of (*a*) poly(vinylpyrrolidinone), (*b*) $Li_x(H_2O)_y(PVP\text{-}10000)_zMoO_3$ and (*c*) hydrated lithium molybdenum bronze

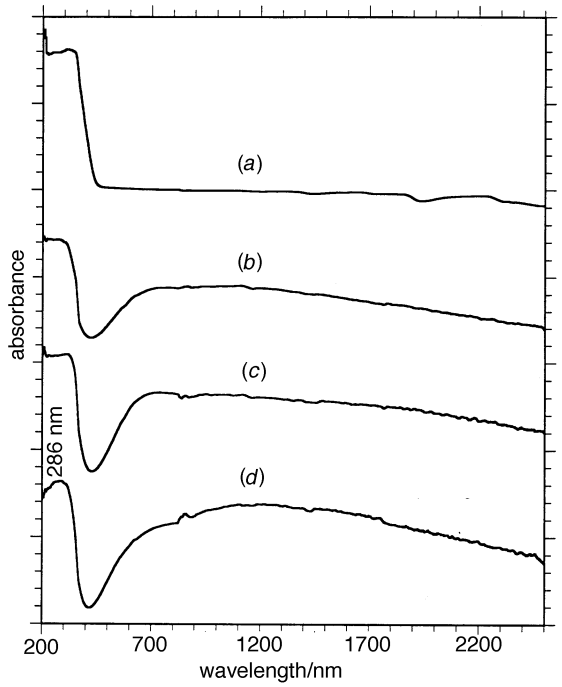

Fig. 3 Solid-state optical absorption spectra of the polymer–Li_xMoO_3 nanocomposites: (*a*) MoO_3, (*b*) $Li_x(H_2O)_yMoO_3$, (*c*) $Li_x(H_2O)_y(PEO\text{-}100\,000)_zMoO_3$, (*d*) $Li_x(H_2O)_y(PAM\text{-}5\,000\,000)_zMoO_3$

of MoO_3 is also demonstrated by X-ray powder diffraction, which shows an expansion of the gallery space. Fig. 4 and 5 show typical XRD patterns of some of the nanocomposites. The sharp and intense (001) reflections indicate that the MoO_3 layers are well stacked. X-Ray scattering coherence lengths, which are calculated from the Scherrer formula $L_{hkl} = K1/b\cos h$,[35] and the gallery spacings are given in Table 1.

The basal spacing of some nanocomposites depends on the preparation procedure. For example, $Li_x(H_2O)_y(PVP)_zMoO_3$, which is water soluble, showed a *d*-spacing of 59.0 Å before washing with isopropyl alcohol and 38.3 Å after washing.

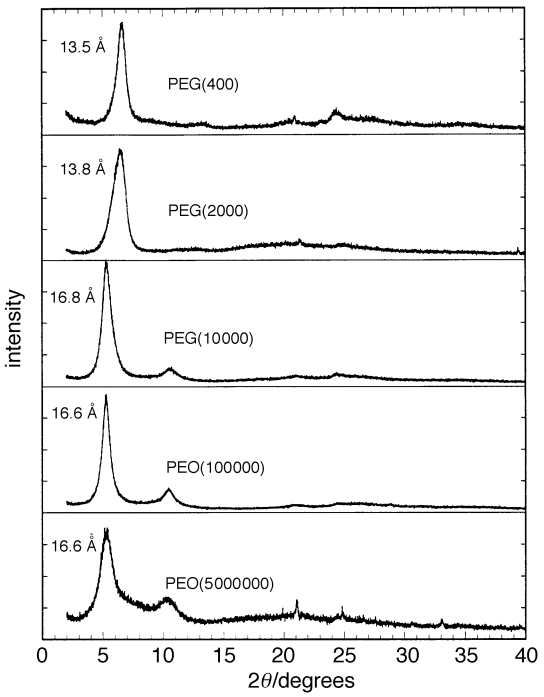

Fig. 4 Typical XRD patterns of nanocomposites with poly(ethylene glycol) and poly(ethylene oxide) of different molecular masses. The polymer and its molecular mass are indicated on each spectrum.

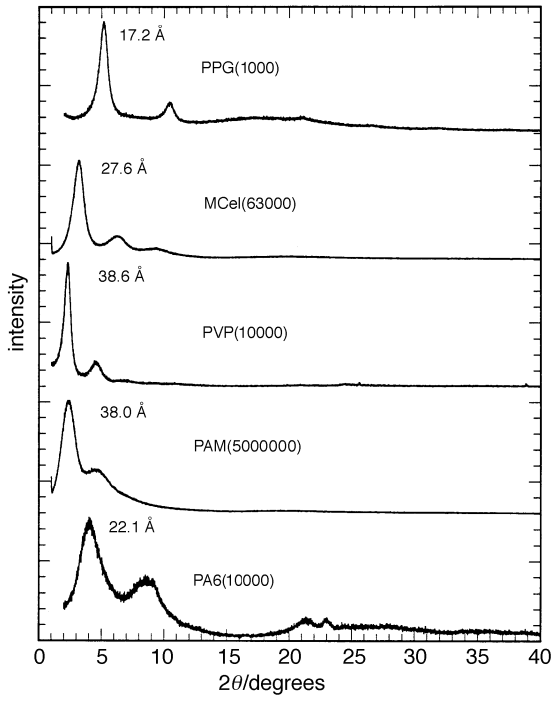

Fig. 5 Typical XRD patterns of the various polymer–Li_xMoO_3 nanocomposites. The polymer and its molecular mass are indicated on each spectrum.

Washing these materials may not only remove extra-lamellar polymer, but could lead to polymer loss from the galleries changing their composition. This behaviour makes it difficult to determine at what polymer loading we begin to saturate the intralamellar space. Similar phenomena were described in polymer–V_2O_5 xerogel systems.[11a] Nevertheless, the observed *d*-spacings were consistent to within ± 1 Å, as long as the preparation procedure was not altered significantly from batch to batch. The *d*-spacings and the degrees of lamellar stacking of products which contained polymers at the very extremes of the molecular mass range (very high or very low) were hard to control, as for example in PEO(5 000 000), PEG(2000) and PPG(1000). The $Li_x(H_2O)_y$(PEO-5 000 000)$_zMoO_3$ had a consistent *d*-spacing of *ca.* 16.6 Å, but the peaks were broad. $Li_x(H_2O)_y$(PEG-2000)$_zMoO_3$ showed broad peaks in the range 12.6–14.7 Å. $Li_x(H_2O)_y$(PPG-1000)$_zMoO_3$ sometimes showed a peak in the range 11.8–17.2 Å, while other samples showed two peaks in this range suggesting a mixture of phases. Evidently, for low molecular masses the polymers are mobile enough in the galleries to form several different arrangements leading to multiple phases.

The effect of polymer molecular mass on product formation was examined, particularly with PEO and PEG, and was found to be significant. The high molecular mass PEO(5 000 000) immediately formed a precipitate with lithium molybdenum bronze in water upon mixing while this phenomenon did not occur with PEO of lower molecular mass. The molecular mass also affects the structure of the nanocomposites. Table 1 shows that the $Li_x(H_2O)_y$(PEO-5 000 000)$_zMoO_3$ sample has a lower coherence scattering length than its lower molecular mass analogues, which is attributed to the fact that it is kinetically unfavourable for extremely long polymer chains to align in an ordered structure. When the molecular mass is extremely low, *i.e.* in oligomer range, the gallery expansion of the intercalate is lower, almost one half of that of the long polymers. For PEO and PEG, a molecular mass of 2000 is about the upper limit of this situation. The data listed in Table 1 show that the $Li_x(H_2O)_y$(PEG-2000)$_zMoO_3$ sample has a much shorter coherence length than its analogues with higher or lower molecular masses. An analogous $Li_x(H_2O)_y$(PEG-2000)$_zMoO_3$ sample, prepared under similar conditions, had a broad X-ray basal peak which corresponded to *d*-spacings varying from 12.6 to 14.7 Å, suggesting that the local conformation of the polymer is important.

Annealing the $Li_x(H_2O)_y$(PEG)$_zMoO_3$ and the $Li_x(H_2O)_y$(PEO)$_zMoO_3$ samples at 150 °C and then gradually cooling them to room temperature tends to improve their lamellar order, especially when the starting coherence length is short. For example, after annealing, the $Li_x(H_2O)_y$(PEG-2000)$_zMoO_3$ sample whose XRD pattern had a broad peak centred at 13.4 Å gave a pattern with a sharp peak at 12.7 Å, (Fig. 6).

The water-insoluble nanocomposite $Li_x(H_2O)_y$(PAM-5 000 000)$_zMoO_3$ gave samples with *d*-spacings of 38.0, 33.8

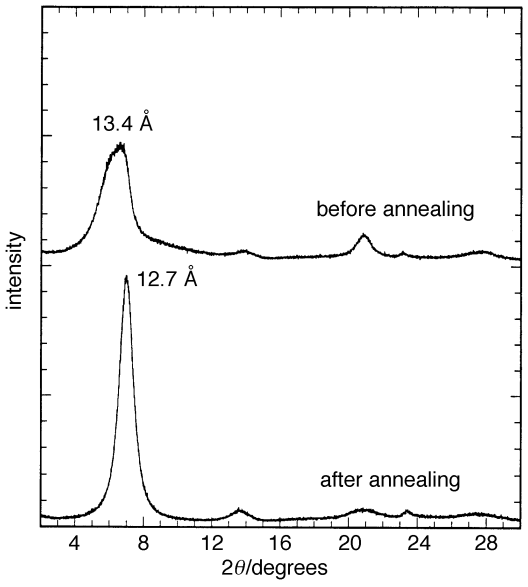

Fig. 6 XRD patterns of $Li_x(H_2O)_y$(PEO-2000)$_zMoO_3$ showing the effect of annealing on the stacking regularity of the layered structure of a nanocomposite

and 41.2 Å. The $Li_x(H_2O)_y(PA6\text{-}10\,000)_zMoO_3$ showed *d*-spacings of 22.1 and 16.8 Å. Occasionally, in the intercalation of PA6 a mixed-phase material with basal spacings of 12.8 and 9.8 Å was obtained. This shows the difficulty in controlling the reaction when quick precipitation is used to obtain a specific phase. To prepare nanocomposites of this type, a very dilute $Li_x(H_2O)_yMoO_3$ suspension of <0.5 mass% is recommended.

The polymer compositions of the nanocomposites were determined by TGA in an oxygen atmosphere and are listed in Table 2. The water in the nanocomposites was estimated by the mass loss step observed below 230 °C, and the amount of polymer was determined by the mass loss steps observed at higher temperatures. Despite drying under vacuum, the nanocomposites retain some water in the galleries. The water-soluble nanocomposites, $Li_x(H_2O)_y(PEO)_zMoO_3$, $Li_x(H_2O)_y(PEG)_zMoO_3$, $Li_x(H_2O)_y(PPG)_zMoO_3$ and $Li_x(H_2O)_y(PVP)_zMoO_3$, usually contain 2–4 mass% water which is very difficult to remove. This water is thought to be coordinated to Li^+ ions. The water-insoluble nanocomposites $Li_x(H_2O)_y(MCel)_zMoO_3$ and $Li_x(H_2O)_y(PAM)_zMoO_3$, however, contain much less water.

Compared to the corresponding polymer–MoS_2 intercalates,[22b] most polymer–Li_xMoO_3 intercalates have much higher polymer contents and larger gallery spacings. As in the polymer–MoS_2 case, PVP and MCel give the largest expansions. A marked difference is found in PAM which gives an expansion as large as 34.3 Å, while PAM–MoS_2, a hybrid prepared by us, has only an expansion of 9.1 Å.[36] This confirms that multiple layers of this polymer can enter the accessible space of Li_xMoO_3.

The water-soluble polymer–Li_xMoO_3 nanocomposites can be cast into films and other shapes, which may provide opportunities for applications. The nanocomposites with high molecular mass polymers are strong, though their mechanical properties depend on the polymer. For example, the nanocomposite of PEO(5 000 000) is tough, while that of PAM(5 000 000) is hard. $Li_x(H_2O)_y(PEO\text{-}5\,000\,000)_zMoO_3$ can be swollen by acetonitrile and becomes resilient and plastic with the consistency of unsulfurized rubber. When the $Li_x(H_2O)_y(PAM\text{-}5\,000\,000)_zMoO_3$ is swollen by water, it is not as plastic, but is stronger and tougher. Precise mechanical measurements have not been taken yet.[37]

Solid-state NMR spectroscopy

In order to probe the effect of the polymer on the behaviour of the lithium ions in the gallery, variable-temperature ^7Li solid-state NMR static spectra were measured for Li_xMoO_3 and $Li_x(H_2O)_y(PEO\text{-}100\,000)_zMoO_3$. In both cases a broad peak was observed with a chemical shift very similar to that of the solid LiCl standard. At −80 °C the lineshapes in the two spectra differ, with that of $Li_x(H_2O)_y(PEO\text{-}100\,000)_zMoO_3$ being slightly more asymmetric, Fig. 7. This suggests that the presence of PEO causes a distribution of Li ions over several, slightly different sites in the gallery. Some of the sites may involve coordination of water molecules while others are associated with the ether-like oxygen atoms of PEO or even those in the MoO_3 layers. The linewidth (width at half maximum) of the resonance peak is greater in the PEO intercalated sample than in the host Li_xMoO_3 material and this too is consistent with a distribution of the Li ions over several sites in the former. The data in the low-temperature region suggest a more well defined coordination environment for the Li ion in Li_xMoO_3 as would be expected in a crystalline solid.

The linewidth of 2300 Hz in Li_xMoO_3 at 23 °C is much narrower than that of *ca.* 12000 Hz observed for $Li_2Mo_2O_4$ indicating a substantial degree of ion motion in the lattice of Li_xMoO_3 relative to that of $Li_2Mo_2O_4$.[38] This is rationalized by the fact that in the latter the Li ions fully occupy well defined crystallographic positions in the lattice[39] while the non-stoichiometric nature of Li_xMoO_3 gives rise to Li mobility *via* vacant crystallographic sites.

The resonance peak in both samples narrows dramatically as the temperature is increased from −80 to 100 °C, Fig. 8. This is attributed to rapid motion of Li ions between the MoO_3 layers. At 100 °C the peak linewidth in the spectra of $Li_x(H_2O)_y(PEO\text{-}100\,000)_zMoO_3$ is comparable to that of $Li_{0.5}(H_2O)_{1.3}Mo_2O_4$.[38] The onset temperature of the transition from a wide to a narrow peak in $Li_x(H_2O)_y(PEO\text{-}100\,000)_zMoO_3$ and Li_xMoO_3 is similar. The spectra of both

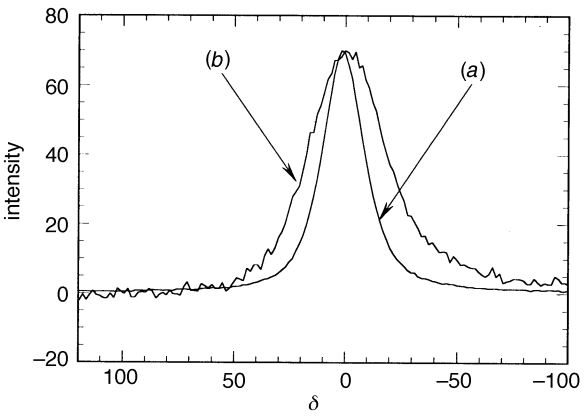

Fig. 7 Static ^7Li NMR spectra of (*a*) Li_xMoO_3 and (*b*) $Li_x(H_2O)_y(PEO\text{-}100\,000)_zMoO_3$ at −80 °C. The broader asymmetric line in the spectrum of the nanocomposite is evident in the upfield region.

Table 2 Composition and physicochemical properties of the polymer–Li_xMoO_3 nanocomposites

nanocomposite	polymer M_w	*d*-spacing/ Å	composition (according to TGA)	limit of thermal stability in N_2/°C	limit of thermal stability in O_2/°C	electronic conductivity/ $S\,cm^{-1}$
pure Li_xMoO_3		8.27				1.3×10^{-2}
pure MoO_3		6.93				3.3×10^{-5}
PEO–Li_xMoO_3	5×10^6	16.6	$Li_{0.25}(H_2O)_{0.20}(PEO)_{0.83}MoO_3$	260	220	2.4×10^{-5}
PEO–Li_xMoO_3	100 000	16.6	$Li_{0.25}(H_2O)_{0.32}(PEO)_{1.04}MoO_3$	260	220	2.9×10^{-5}
PEG–Li_xMoO_3	10 000	16.8	$Li_{0.25}(H_2O)_{0.29}(PEG)_{0.75}MoO_3$	260	220	5.2×10^{-5}
PEG–Li_xMoO_3	2000	13.8	$Li_{0.25}(H_2O)_{0.28}(PEG)_{0.57}MoO_3$	260	220	2.2×10^{-4}
PEG–Li_xMoO_3	400	13.5	$Li_{0.25}(H_2O)_{0.38}(PEG)_{0.33}MoO_3$	260	220	3.1×10^{-4}
PPG–Li_xMoO_3	1000	17.2	$Li_{0.25}(H_2O)_{0.18}(PPG)_{0.99}MoO_3$	220	200	—
		11.8	$Li_{0.25}(H_2O)_{0.52}(PPG)_{0.14}MoO_3$			5.3×10^{-4}
MCel–Li_xMoO_3	63 000	27.6	$Li_{0.25}(MCel)_{0.70}MoO_3$	180	170	2.0×10^{-6}
PVP–Li_xMoO_3	10 000	38.6	$Li_{0.25}(H_2O)_{0.43}(PVP)_{1.17}MoO_3$	220	220	1.8×10^{-7}
PAM–Li_xMoO_3	5×10^6	38.0	$Li_{0.25}(PAM)_{3.2}MoO_3$	150	150	6.3×10^{-7}
PA6–Li_xMoO_3	10 000	22.1	$Li_{0.25}(H_2O)_{0.44}(PA6)_{0.32}MoO_3$	280	270	—
		16.8	$Li_{0.25}(H_2O)_{0.48}(PA6)_{0.32}MoO_3$			2.1×10^{-4}

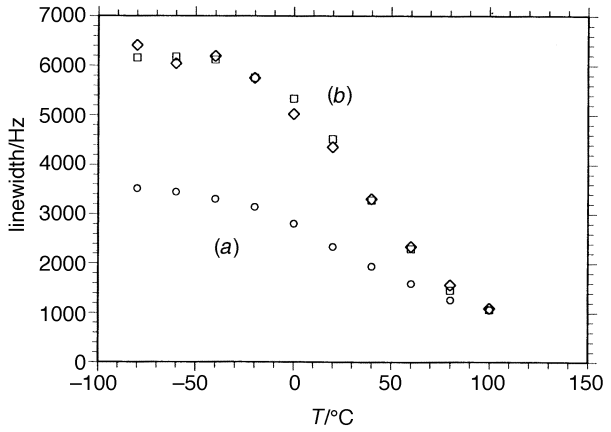

Fig. 8 Temperature dependence of the linewidth of the resonance peak in the solid-state ^{7}Li NMR spectra of (*a*) Li_xMoO_3 and (*b*) $Li_x(H_2O)_y(PEO\text{-}100\,000)_zMoO_3$

materials end up with an equally narrow peak at 100 °C indicating comparable rates of hopping of Li ions between different positions in the interior of the two materials.

Preliminary solid-state, cross-polarization, magic angle spinning ^{13}C NMR spectra, as a function of temperature, suggest a substantial degree of motion in the polymer backbone as well. At room temperature a single broad resonance is observed for the $-CH_2-$ group at d 71.6, with a linewidth of 1380 Hz. As the temperature rises, the resonance does not shift but it narrows dramatically and at 80 °C it is only 200 Hz, consistent with rapid thermal motion of the polymer chains. This motion should facilitate the hopping of Li ions in the gallery and contribute to a high ionic conductivity for the material.

Magnetism

Because the materials are formally mixed-valence compounds and exhibit intense intervalence Mo^{5+}–Mo^{6+} optical transitions, we expect unpaired electrons to be delocalized over the d orbitals of the Mo atoms. Magnetic susceptibility measurements were carried out as a function of temperature for Li_xMoO_3 and $Li_x(H_2O)_y(PEO\text{-}100\,000)_zMoO_3$ and the data are displayed in Fig. 9. Surprisingly, the susceptibility of both these compounds is rather small with substantial contributions from temperature independent paramagnetism (x_{TIP}). Correcting for the latter, $1/(x_{molar}-x_{TIP})$ *vs.* T plots for Li_xMoO_3 and $Li_x(H_2O)_y(PEO\text{-}100\,000)_zMoO_3$ are linear in the temperature ranges 5–120 K and 2–300 K, respectively. The Curie constants estimated from the slope of the plots yield μ_{eff} of 0.15 and 0.09 respectively, however, the weak susceptibilities and the large diamagnetic and x_{TIP} corrections make μ_{eff} values unreliable. It is interesting that the magnetic properties

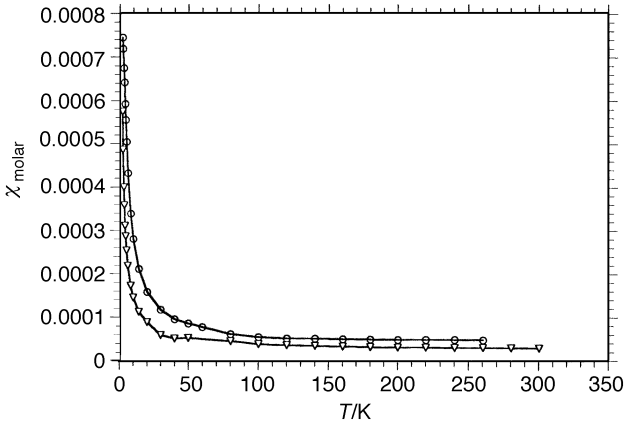

Fig. 9 Temperature dependence of magnetic susceptibility of Li_xMoO_3 (#) and $Li_x(H_2O)_y(PEO\text{-}100\,000)_zMoO_3$ (′). The measurements were conducted at 1000 G with powder samples.

of Li_xMoO_3 are more similar to those of $Li_{0.9}Mo_6O_{17}$[40] than of other molybdenum bronzes such as the blue bronze $A_{0.3}MoO_3$ (A = K, Tl) and purple bronzes $A_{0.9}Mo_6O_{17}$ (A = K, Na, Tl).[41–44] In the latter bronzes the temperature dependence of the magnetic susceptibility shows transitions at low temperature associated with charge density waves. Such phenomena were not observed in the Li_xMoO_3 samples reported here.

Electrical conductivity

Electrical conductivity values for all the nanocomposites are listed in Table 2. The room-temperature electrical conductivity of Li_xMoO_3 was 0.013 S cm^{-1} which is slightly lower than values reported in related materials.[45,46] As shown in Table 2, the conductivity of the nanocomposites is significantly lower than that of Li_xMoO_3 and decreases with increasing layer expansion. For materials with extremely large gallery spacing, the electrical conductivity is lower than that of MoO_3 itself. When the measurements are performed under vacuum the conductivity decreases concomitantly with the loss of water from the galleries. This suggests that water is contributing to charge transport in these materials probably *via* proton mobility. Fig. 10 shows the temperature dependence of the electrical conductivity of Li_xMoO_3 and $Li_x(H_2O)_y(PEO\text{-}100\,000)_zMoO_3$, which is thermally activated. Mixed ionic/electronic conducting nanocomposites are of current interest.[12]

Conclusion

A new family of polymer–molybdenum bronze nanocomposites has been synthesized. The host material, Li_xMoO_3, was synthesized *via* a $LiBH_4$ route which is different from the conventional approach. This material exfoliates in water and has affinity for a large variety of polymers. Polymers such as PEG, PEO, PPG, PVP, MCel, PAM and PA6 give well stacked lamellar nanocomposites. Depending on the nature of

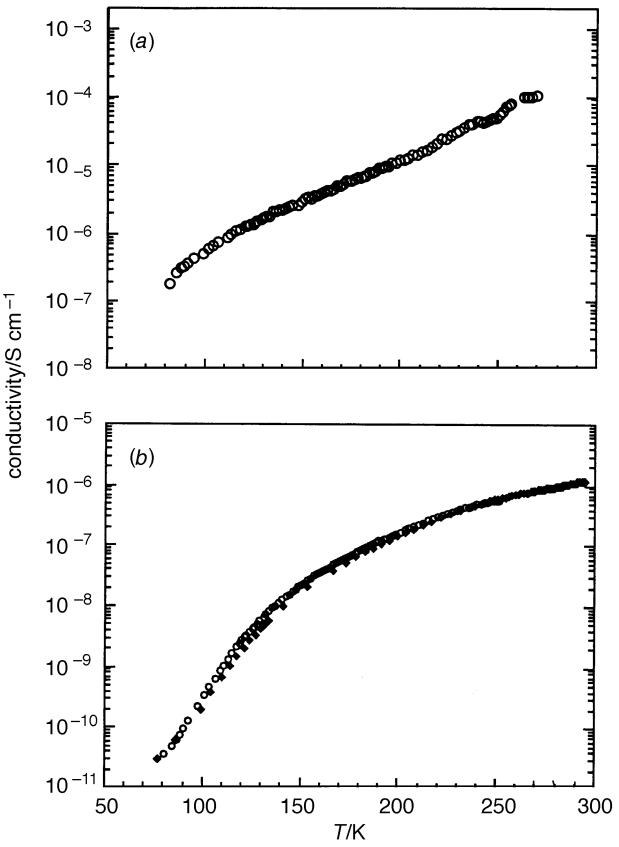

Fig. 10 Variable-temperature electrical conductivity measurements for pressed pellet samples of (*a*) Li_xMoO_3 and (*b*) $Li_x(H_2O)_y(PEO\text{-}100000)_zMoO_3$

the polymer and its molecular mass, some of the nanocomposites are soluble and can be processed into films. Electronic transmission spectra show the broad transition associated with the Mo^{5+}–Mo^{6+} couple in these nanocomposites ranging from the IR to the visible region. Solid-state ^7Li NMR spectroscopy indicates a more versatile chemical environment in the nanocomposites than in the host which may lead to high ionic conductivities in these lamellar systems. The electrical conductivity of these materials is thermally activated and ranges from 10^{-2} to 10^{-7} S cm^{-1}.

Financial support from the National Science Foundation (DMR-93-06385) is gratefully acknowledged. This work made use of the NMR facilities of the Department of Chemistry and magnetic measurements facilities of the Department of Physics at Michigan State University. At Northwestern University this work made use of Central Facilities supported by NSF through the Materials Research Center (DMR-91-20521). We thank Kermit Johnson for assistance with the Li NMR spectroscopy.

References

1 (*a*) Y. Fukushima and S. Inagaki, *J. Inclusion Phenom.*, 1987, **5**, 473; (*b*) Y. Fukushima, A. Okada, M. Kawasumi, T. Kurauchi and O. Kamigaito, *Clay Miner.*, 1988, **23**, 27; (*c*) A. Usuki, M. Kawasumi, Y. Kojima, A. Okada, T. Kurauchi and O. Kamigaito, *J. Mater. Res.*, 1993, **8**, 1174; (*d*) A. Usuki, Y. Kojima, M. Kawasumi, A. Okada, Y. Fukushima, T. Kurauchi and O. Kamigaito, *J. Mater. Res.*, 1993, **8**, 1179; (*e*) Y. Kojima, A. Usuki, M. Kawasumi, A. Okada, Y. Fukushima, T. Kurauchi and O. Kamigaito, *J. Mater. Res.*, 1993, **8**, 1185.

2 (*a*) E. P. Giannelis, *Adv. Mater.*, 1996, **8**, 29; (*b*) R. Krishnamoorti, R. A. Vaia and E. P. Giannelis, *Chem. Mater.*, 1996, **8**, 1728; (*c*) E. P. Giannelis, V. Mehrotra, O. Tse, R. A. Vaia and T.-C. Sung, *Mater. Res. Soc. Symp. Proc.*, 1992, **267**, 969; (*d*) R. A. Vaia, H. Ishii and E. P. Giannelis, *Chem. Mater.*, 1993, **5**, 1694; (*e*) R. A. Vaia, S. Vasudevan, W. Krawiec, L. G. Scanlon and E. P. Giannelis, *Adv. Mater.*, 1995, **7**, 154; (*f*) S. D. Burnside and E. P. Giannelis, *Chem. Mater.*, 1995, **7**, 1597; (*g*) R. A. Vaia, K. D. Jandt, E. J. Kramer and E. P. Giannelis, *Macromolecules*, 1995, **28**, 8080; (*h*) P. B. Messersmith and E. P. Giannelis, *J. Polym. Sci., Part A: Polym. Chem.*, 1995, **33**, 1047; (*i*) P. B. Messersmith and E. P. Giannelis, *Chem. Mater.*, 1993, **5**, 1064; (*j*) 1994, **6**, 1719.

3 (*a*) M. S. Wang and T. J. Pinnavaia, *Chem. Mater.*, 1994, **6**, 468; (*b*) T. Lan, P. D. Kaviratna and T. J. Pinnavaia, *Chem. Mater.*, 1994, **6**, 573; (*c*) T. Lan and T. J. Pinnavaia, *Chem. Mater.*, 1994, **6**, 2216; (*d*) H. Shi, T. Lan and T. J. Pinnavaia, *Chem. Mater.*, 1996, **8**, 1584; (*e*) Z. Wang, T. Lan and T. J. Pinnavaia, *Chem. Mater.*, 1996, **8**, 2200; (*f*) T. Lan, D. Kaviratna and T. J. Pinnavaia, *J. Phys. Chem. Solids*, 1996, **57**, 1005.

4 (*a*) E. Ruiz-Hitzky and P. Aranda, *Adv. Mater.*, 1990, **2**, 545; (*b*) P. Aranda and E. Ruiz-Hitzky, *Chem. Mater.*, 1992, **4**, 1395.

5 M. Iwai, H. Shoji, S. Shimazu and T. Uematsu, *Chem. Lett.*, 1993, 403.

6 T. Kyotani, T. Mori and A. Tomita, *Chem. Mater.*, 1994, **6**, 2138.

7 J. J. Tunney and C. Detellier, *Chem. Mater.*, 1996, **8**, 927.

8 J. C. Hutchison, R. Bissessur and D. F. Shriver, *Chem. Mater.*, 1996, **8**, 1597.

9 Y. Kurokawa, H. Yasuda and A. Oya, *J. Mater. Sci. Lett.*, 1996, **15**, 1481.

10 (*a*) M. G. Kanatzidis, L. M. Tonge, T. J. Marks, H. O. Marcy and C. R. Kannewurf, *J. Am. Chem. Soc.*, 1987, **109**, 3797; (*b*) M. G. Kanatzidis, H. O. Marcy, W. J. McCarthy, C. R. Kannewurf and T. J. Marks, *Solid State Ionics*, 1989, **32/33**, 594; (*c*) M. G. Kanatzidis, C.-G. Wu, H. O. Marcy, D. C. DeGroot, C. R. Kannewurf, A. Kostikas and V. Papaefthymiou, *Adv. Mater.*, 1990, **2**, 364; (*d*) C.-G. Wu, H. O. Marcy, D. C. DeGroot, J. L. Schindler, C. R. Kannewurf, W.-Y. Leung, M. Benz, E. LeGoff and M. G. Kanatzidis, *Synth. Met.*, 1991, **41–43**, 797; (*e*) M. G. Kanatzidis, C.-G. Wu, D. C. DeGroot, J. L. Schindler, M. Benz, E. LeGoff and C. R. Kannewurf, in *Chemical Physics of Intercalation II*, ed. J. Fisher, NATO ASI Ser., Plenum, 1993, p. 63.

11 (*a*) Y.-J. Liu, D. C. DeGroot, J. L. Schindler, C. R. Kannewurf and M. G. Kanatzidis, *Chem. Mater.*, 1991, **3**, 992; (*b*) Y.-J. Liu, D. C. DeGroot, J. L. Schindler, C. R. Kannewurf and M. G. Kanatzidis, *Adv. Mater.*, 1993, **5**, 369; (*c*) Y.-J. Liu, J. L. Schindler, D. C. DeGroot, C. R. Kannewurf, W. Hirpo and M. G. Kanatzidis, *Chem. Mater.*, 1996, **8**, 525; (*d*) C.-G. Wu, M. G. Kanatzidis, H. O. Marcy, D. C. DeGroot and C. R. Kannewurf, in *Lower-Dimensional Systems and Molecular Electronics*, ed. R. M. Metzger, *et al.*, Plenum, New York, 1991, p. 427; (*e*) Y.-J. Liu, D. C. DeGroot, J. L. Schindler, C. R. Kannewurf and M. G. Kanatzidis, *J. Chem. Soc., Chem. Commun.*, 1993, 593; (*f*) C.-G. Wu, D. C. DeGroot, H. O. Marcy, J. L. Schindler, C. R. Kannewurf, Y.-J. Liu, W. Hirpo and M. G. Kanatzidis, *Chem. Mater.*, 1996, **8**, 1992.

12 G. M. Kloster, J. A. Thomas, P. W. Brazis, C. R. Kannewurf and D. F. Shriver, *Chem. Mater.*, 1996, **8**, 2418.

13 F. Leroux, B. E. Koene and L. F. Nazar, *J. Electrochem. Soc.*, 1996, **143**, L181.

14 (*a*) L. F. Nazar, X. T. Yin, D. Zinkweg, Z. Zhang and S. Liblong, *Mater. Res. Soc. Symp. Proc.*, 1991, **210**, 417; (*b*) L. F. Nazar, Z. Zhang and D. Zinkweg, *J. Am. Chem. Soc.*, 1992, **114**, 6239; (*c*) L. F. Nazar, H. Wu and W. P. Power, *J. Mater. Chem.*, 1995, **5**, 1985; (*d*) T. A. Kerr, H. Wu and L. F. Nazar, *Chem. Mater.*, 1996, **8**, 2005.

15 R. Bissessur, D. C. DeGroot, J. L. Schindler, C. R. Kannewurf and M. G. Kanatzidis, *J. Chem. Soc., Chem. Commun.*, 1993, 687.

16 G. Cao and T. E. Mallouk, *J. Solid State Chem.*, 1991, **94**, 59.

17 J. E. Pillion and M. E. Thompson, *Chem. Mater.*, 1991, **3**, 777.

18 A. Clearfield and C. Y. Ortiz-Avila, in *ACS Symposium 499: Supramolecular Architecture*, ed. T. Bein, American Chemical Society, 1992, p. 178.

19 Y.-J. Liu and M. G. Kanatzidis, *Inorg. Chem.*, 1993, **32**, 2989.

20 Y. Ding, D. J. Jones, P. Maireles-Torres and J. Rozière, *Chem. Mater.*, 1995, **7**, 562.

21 W. M. R. Divigalpitiya, R. F. Frindt and S. R. Morrison, *J. Mater. Res.*, 1991, **6**, 1103.

22 (*a*) M. G. Kanatzidis, R. Bissessur, D. C. DeGroot, J. L. Schindler and C. R. Kannewurf, *Chem. Mater.*, 1993, **5**, 595; (*b*) R. Bissessur, M. G. Kanatzidis, J. L. Schindler and C. R. Kannewurf, *J. Chem. Soc., Chem. Commun.*, 1993, 1582; (*c*) R. Bissessur, J. L. Schindler, C. R. Kannewurf and M. G. Kanatzidis, *Mol. Cryst. Liq. Cryst.*, 1993, **245**, 249; (*d*) L. Wang, J. L. Schindler, J. A. Thomas, C. R. Kannewurf and M. G. Kanatzidis, *Chem. Mater.*, 1995, **7**, 1753.

23 J. P. Lemmon and M. M. Lerner, *Chem. Mater.*, 1994, **6**, 207.

24 E. Ruiz-Hitzky, R. Jimenez, B. Casal, V. Manriquez, A. S. Ana and G. Gonzalez, *Adv. Mater.*, 1993, **5**, 738.

25 I. Lagadic, A. Léaustic and R. Clément, *J. Chem. Soc., Chem. Commun.*, 1992, 1396.

26 C. O. Oriakhi and M. M. Lerner, *Chem. Mater.*, 1996, **8**, 2016.

27 P. G. Hill, P. J. S. Foot and R. Davis, *Synth. Met.*, 1996, **76**, 289.

28 P. B. Messersmith and S. I. Stupp, *Chem. Mater.*, 1995, **7**, 454.

29 H.-L. Tsai, J. Heising, J. L. Schindler, C. R. Kannewurf and M. G. Kanatzidis, to be published.

30 N. Margalit, *J. Electrochem. Soc.*, 1974, **121**, 1460.

31 J. Desilvestro and O. Haas, *J. Electrochem. Soc.*, 1990, **137**, 5C.

32 M. G. Kanatzidis and T. J. Marks, *Inorg. Chem.*, 1987, **26**, 783.

33 (*a*) B. N. Diel, T. Inabe, J. W. Lyding, K. F. Schock Jr., C. R. Kannewurf and T. J. Marks, *J. Am. Chem. Soc.*, 1983, **105**, 1551; (*b*) J. W. Lyding, H. O. Marcy, T. J. Mark and C. R. Kannewurf, *IEEE Trans. Instrum. Meas.* 1988, **37**, 76.

34 D. M. Thomas and E. M. McCarron III, *Mater. Res. Bull.*, 1986, **21**, 945.

35 D. M. Moore and R. C. Reynolds Jr., *X-Ray Diffraction and the Identification and Analysis of Clay Minerals*, Oxford University Press, Oxford and New York, 1989, p. 83.

36 L. Wang and M. G. Kanatzidis, unpublished work.

37 L. Wang and M. G. Kanatzidis, work in progress.

38 S. Colson, J. M. Tarascon, S. Szu and L. C. Klein, *Mater. Res. Soc. Symp. Proc.*, 1991, **210**, 405.

39 J. M. Tarascon and S. Colson, *Mater. Res. Soc. Symp. Proc.*, 1989, **135**, 421.

40 Y. Matsuda, M. Sato, M. Onoda and K. Nakao, *J. Phys. C: Solid State Phys.*, 1986, **19**, 6039.

41 M. Greenblatt, in *Low-Dimensional Electronic Properties of Molybdenum Bronzes and Oxides*, ed. C. Schlenker, Kluwer Academic, Dordrecht, Boston, London, 1989.

42 L. F. Schneemeyer, F. J. DiSalvo, R. M. Fleming and J. V. Waszczak, *J. Solid State Chem.*, 1984, **54**, 358.

43 G. H. Bouchard Jr., J. Perlstein and M. J. Sienko, *Inorg. Chem.*, 1967, **6**, 1682.

44 D. C. Johnston, *Phys. Rev. Lett.*, 1984, **52**, 2049.

45 C. Julien and G. A. Nazri, *Solid State Ionics*, 1994, **68**, 111.

46 J. O. Besenhard, J. Heydecke, E. Wudy and H. P. Fritz, *Solid State Ionics*, 1983, **8**, 61.

Paper 7/00202E; *Received* 8*th January*, 1997